HeRCULES: Heterogeneous Radar Dataset in Complex Urban Environment for Multi-session Radar SLAM

Hanjun Kim[1], Minwoo Jung[2], Chiyun Noh[2], Sangwoo Jung[2],
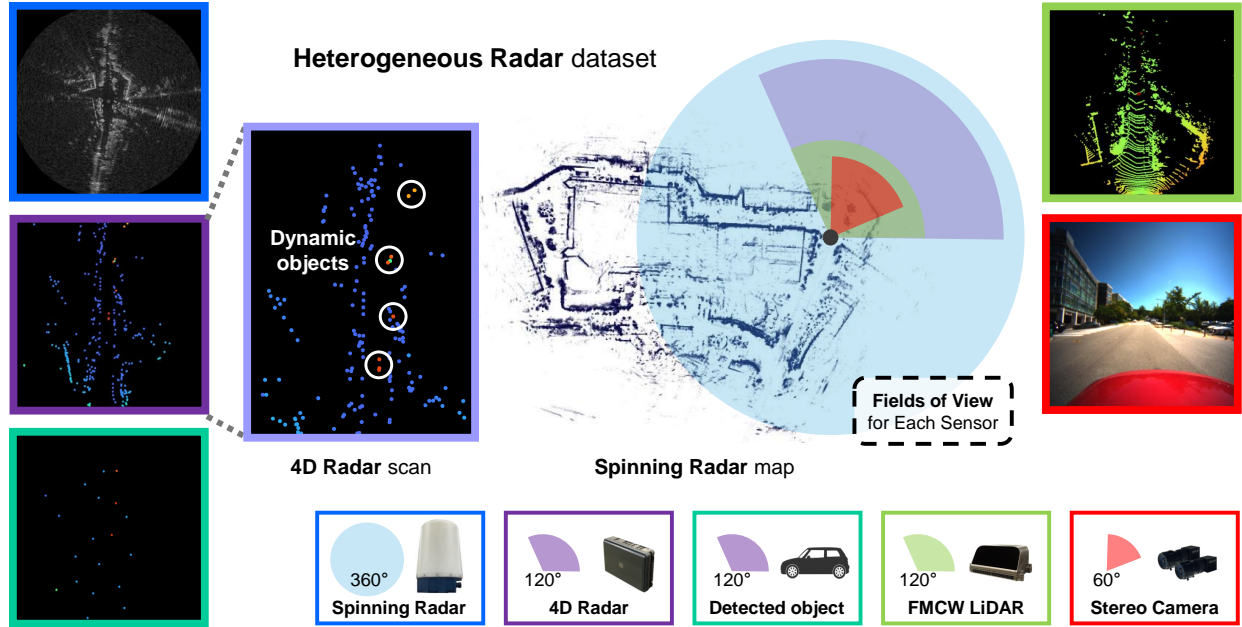Hyunho Song[2], Wooseong Yang[2], Hyesu Jang[2] and Ayoung Kim[2*]

Fig. 1: Overview of the HeRCULES Dataset. The FMCW LiDAR and 4D radar point colors represent relative velocities, with red indicating objects moving away and blue indicating objects approaching. Colors are normalized for each image to enhance visibility.

Abstract— Recently, radars have been widely featured in robotics for their robustness in challenging weather conditions. Two commonly used radar types are spinning radars and phased-array radars, each offering distinct sensor characteristics. Existing datasets typically feature only a single type of radar, leading to the development of algorithms limited to that specific kind. In this work, we highlight that combining different radar types offers complementary advantages, which can be leveraged through a heterogeneous radar dataset. Moreover, this new dataset fosters research in multi-session and multi-robot scenarios where robots are equipped with different types of radars. In this context, we introduce the HeRCULES dataset, a comprehensive, multi-modal dataset with heterogeneous radars, FMCW LiDAR, IMU, GPS, and cameras. This is the first dataset to integrate 4D radar and spinning radar alongside FMCW LiDAR, offering unparalleled localization, mapping, and place recognition capabilities. The dataset covers diverse weather and lighting conditions and a range of urban traffic scenarios, enabling a comprehensive analysis across various environments. The sequence paths with multiple revisits and ground truth pose for each sensor enhance its suitability for place recognition research. We expect the HeRCULES dataset to facilitate odometry, mapping, place recognition, and sensor fusion research. The dataset and development tools are available at **https://sites.google.com/view/herculesdataset**.

I. INTRODUCTION

Recently, radar has gained significant attention for its reliable performance in conditions such as fog, rain, and low-light environments. Consequently, various radars with different operating modes and unique characteristics have been introduced [1]. For example, spinning radar, also known as scanning or imaging radar, offers 360° coverage, a longer perceptible range, and is more resistant to occlusion, making it effective for place recognition or odometry estimation [2–4]. Another widely utilized radar in robotics, phased-array radar, also referred to as system-on-a-chip (SoC) radar, is lightweight and consumes less power, making it ideal for object tracking in autonomous vehicles [5–7]. More recently, 4D Frequency Modulated Continuous Wave (FMCW) radar, which provides elevation information in addition to azimuth and range, has been widely adopted in object detection and simultaneous localization and mapping (SLAM) [8–12].

Despite these advancements in radar systems, research integrating multiple types of radars remains less explored. While some datasets and studies have utilized multi-radar se-

[1]H. Kim is with the Dept. of Future Automotive Mobility, SNU, Seoul, S. Korea hanjun815@snu.ac.kr

[2]M. Jung, C. Noh, S. Jung, H. Song, W. Yang, H. Jang and A. Kim are with the Dept. of Mechanical Engineering, SNU, Seoul, S. Korea [moonshot, gch06208, dan0130, hun1021405, yellowish, dortz, ayoungk]@snu.ac.kr

TABLE I: COMPARISON WITH EXISTING RADAR DATASETS

Radar	Dataset	Camera	Radar		LiDAR	IMU	GPS	Size	ROS Support	Condition	Scenarios
			4D Radar	Scanning Radar							
4D Radar	Astyx [13]	Mono	Astyx 6455 HiRes	-	3D	-	-	small	-	-	suburban
	RADIal [14]	Mono	Valeo DDM	-	3D	-	RTK	medium	-	-	urban, rural
	View-of-Delft [15]	Stereo	ZF FRGen21	-	3D	✓	RTK	medium	-	-	urban
	TJ4DRadSet [16]	Mono	Oculii Eagle	-	3D	-	RTK	medium	✓	night	urban
	K-Radar [17]	Stereo	RETINA-4ST	-	3D	✓	RTK	large	-	night, fog, rain, snow	urban, suburban, campus, mountain, alleyway
	MSC-RAD4R [18]	Stereo	Oculii Eagle	-	3D	✓	RTK	medium	✓	night, smoke, rain	urban, rural, tunnel, campus, alleyway
	NTU4DRadLM [19]	Mono	Oculii Eagle	-	3D	✓	RTK	medium	✓	night	campus
	Dual Radar [20]	Mono	Continental ARS548, Arbe Phoenix	-	3D	✓	-	large	-	night, dusk, rain	urban, tunnel
	Snail radar [21]	Stereo	Continental ARS548, Oculii Eagle	-	3D	✓	RTK	large	✓	night, dusk, rain	campus, highway, tunnels, overpass
Scanning Radar	Oxford Radar [22]	Stereo	-	Navtech CTS350-X	3D	-	GPS	large	-	rain	urban
	MulRan [23]	-	-	Navtech CIR204-H	3D	✓	RTK	medium	✓	-	urban, tunnel, campus
	RADIATE [24]	Stereo	-	Navtech CTS350-X	3D	✓	GPS	medium	-	night, fog, rain, snow	urban, park
	Boreas [25]	Mono	-	Navtech CIR304-H	3D	✓	RTX	large	-	night, rain, snow	urban
	OORD [26]	Mono	-	Navtech CTS350-X	3D	✓	GPS	medium	-	night, snow	offroad
Heterogeneous Radar	**HeRCULES**	**Stereo**	**Continental ARS548**	**Navtech RAS6**	**4D**	✓	**RTK**	**large**	✓	**night, dusk, rain, snow**	**urban, bridge, campus, mountain, stream, alleyway**

tups, they have all featured homogeneous radars [20, 21, 27]. This highlights a gap in existing resources, particularly compared to research on heterogeneous radar systems.

To address this gap, we introduce the HeRCULES dataset—Heterogeneous Radar dataset in Complex Urban environment for muLti-sEssion radar SLAM—designed to capture rich spatial and velocity information through the combination of heterogeneous radars. This is the first dataset to integrate both 4D radar and spinning radar alongside FMCW Light Detection and Ranging (LiDAR), inertial measurement unit (IMU), RTK-GPS, and cameras, as shown in Fig. 1 and Fig. 2. Instead of using a conventional 3D spinning LiDAR, we utilize FMCW LiDAR, which leverages the advantages of the latest FMCW radar by adopting FMCW signal methods rather than traditional pulsed laser signals [28–30]. This unique setup enables direct comparisons between 4D radar and FMCW LiDAR, supporting research in radar-LiDAR fusion SLAM and cross-sensor place recognition. Furthermore, we believe the provided sequences are particularly ideal for multi-session SLAM using this heterogeneous sensor setup.

The HeRCULES dataset encompasses various weather and lighting conditions, diverse traffic scenarios, and environments with a large number of dynamic objects. The sequence paths are designed to include multiple revisits to the same locations to support place recognition research. We provide a Robot Operating System (ROS) player and radar format conversion software to facilitate easy integration with existing place recognition and SLAM tools. Additionally, the dataset offers ground truth pose for each sensor and presents benchmark evaluations for SLAM and place recognition tasks, ensuring comprehensive validation.

Our main contributions are as follows:

- The HeRCULES dataset is the first public dataset, including both a 4D radar and a scanning radar, providing capabilities for localization, mapping, and place recognition. Moreover, it incorporates the latest FMCW LiDAR with 4D radar, uniquely suited for radar-LiDAR fusion SLAM and cross-sensor place recognition.
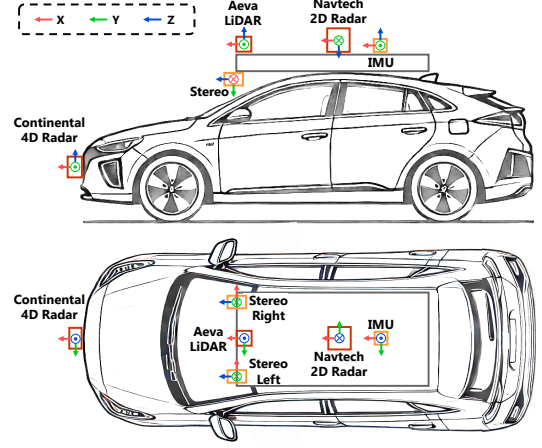

Fig. 2: Sensor overview of HeRCULES and coordinate of sensors. The x, y, and z coordinates are red, green, and blue.

- The HeRCULES dataset encompasses various weather and lighting conditions, a range of traffic scenarios, and environments with a large number of dynamic objects. The dataset covers an extensive area, enabling comprehensive analysis across various environments.
- We have designed the sequence paths to include multiple revisits to the same locations. This ensures sufficient queries for place recognition and multi-session SLAM.
- We provide a ROS player, radar format conversion software for integration with existing place recognition and SLAM tools, and ground truth poses for each sensor to support place recognition research.

II. RELATED WORK

A. The Dataset with 4D Radar

4D radar captures range, azimuth, elevation, Radar Cross Section (RCS), and Doppler velocity, enhancing perception capabilities in dynamic scenarios. While Astyx [13] was pioneering in using 4D radar for object detection, its limited diversity and lack of localization references restrict broader applications. Similarly, RADIal [14] offers multi-modal data

TABLE II: SENSOR SPECIFICATIONS

Sensor	Type	Data type	Resolution			FOV			Frequency
			Range	Azimuth	Elevation	Range	Azimuth	Elevation	
4D Radar	Continental ARS548	x, y, z, velocity, RCS, range, azimuth, elavation	0.22 m	1.2°@0. . . ±15° 1.68°@ ±45°	2.3°	300 m	±60°	±4°@300 m ±14°@<100 m	20 Hz
Spinning Radar	Navtech RAS6	Polar image, Cartesian image	0.044 m	0.9°	-	330 m	360°	-	4 Hz
FMCW LiDAR	Aeva Aries II	x, y, z, reflectivity, intensity, velocity, line-index, time-offset	0.02 m@1σ	0.025°	0.025°	150 m	120°	30°	10 Hz
Camera	FLIR Blackfly S BFS-U3-16S2C-CS USB3	8-bit Bayer pattern png format	-	1440 px	1080 px	-	60°	45°	15 Hz
IMU	Xsens MTi-300	q_x, q_y, q_z, q_w, eul_x, eul_y, eul_z, gyr_x, gyr_y, gyr_z, acc_x, acc_y, acc_z, mag_x, mag_y, mag_z	-	-	-	-	-	-	100 Hz
RTK-GPS	Hexagon NovAtel SPAN-CPT7	latitude, longitude, height, $velocity_{north}$, $velocity_{east}$, $velocity_{up}$, roll, pitch, azimuth, status	-	-	-	-	-	-	50 Hz

for urban environments but lacks varied environmental conditions and does not include an IMU, relying instead on mono camera setups. View-of-Delft [15] incorporates global positioning system (GPS), IMU, 4D radar, cameras, and LiDAR for object detection and tracking. However, its radar is limited to short-range and lacks long-range 4D radar data. The TJ4DRadSet dataset [16] focuses on object detection and tracking but excludes adverse weather conditions and lacks an IMU. K-Radar [17] offers a large-scale 4D radar dataset across various weather conditions but only includes a 6-axis IMU integrated within the LiDAR and lacks radar point cloud data. MSC-RAD4R [18] includes stereo cameras, LiDAR, RTK-GPS, and IMU data over 51.6 km but suffers from significant RTK closure errors in height and incorrect headings from the Attitude and Heading Reference System (AHRS) system. NTU4DRadLM [19] is limited in diverse weather conditions, reducing its effectiveness for robust SLAM research. Although Dual Radar [20] and Snail Radar [21] feature dual radar systems and diverse environments, they only utilize homogeneous radars.

The HeRCULES dataset is the first to combine 4D radar, spinning radar, FMCW LiDAR, cameras, IMU, and RTK-GPS. Unlike other datasets, HeRCULES provides not only the radar point cloud data from the 4D radar but also the object point cloud information filtered through the object filtering process of the ars548 RDI radar driver[1].

B. The Dataset with Spinning Radar

Spinning radar provides detailed 360° long-range scans, essential for mapping and localization in complex environments. While the Oxford Radar RobotCar Dataset [22] and MulRan [23] offer valuable data for place recognition and localization in urban settings, they are limited in scope and sensor diversity. The Oxford Radar RobotCar Dataset is restricted to urban areas and lacks scenarios in diverse environments like mountains and river bridges. It also does not include IMU, RTK-GPS, and nighttime data. Similarly, MulRan lacks camera data and does not cover varied weather and lighting conditions. The RADIATE [24] and Boreas [25] datasets focus on adverse weather and multi-seasonal environments. However, RADIATE lacks sufficient repeated traversals necessary for robust place recognition tasks. Despite offering a broader range of conditions, Boreas is limited
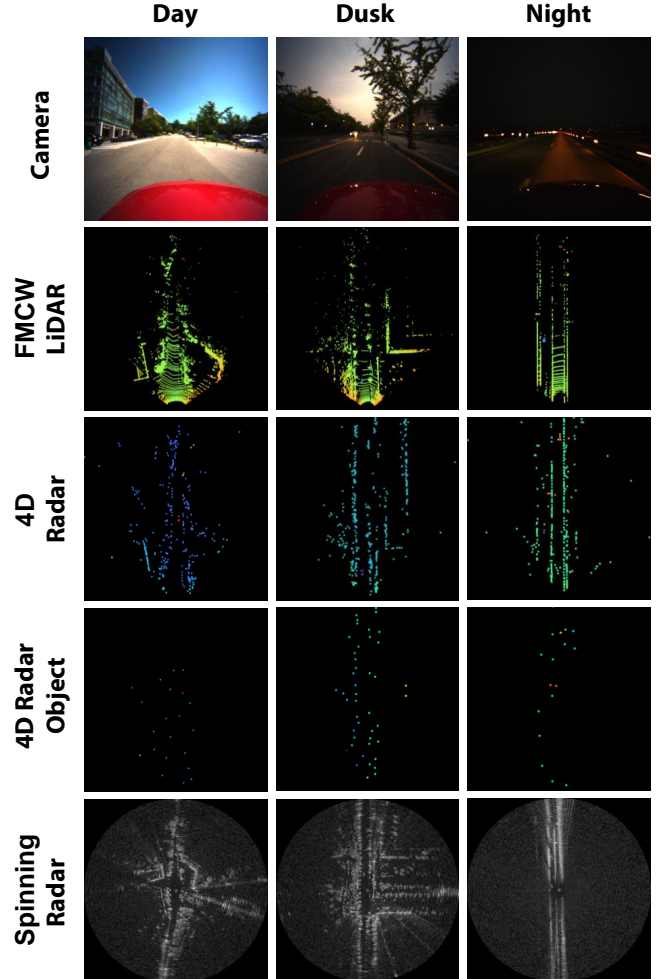

Fig. 3: Day, dusk, and night conditions of the HeRCULES dataset.

to relatively flat urban and suburban terrains, lacking the complexity of more varied landscapes. The Oxford Offroad Radar Dataset (OORD) [26] features challenging off-road environments but lacks a comprehensive range of urban and rural scenarios.

Compared to existing datasets, the HeRCULES dataset offers several key advantages, as shown in Table. I. All the above datasets are limited to 2D radar and do not provide Doppler velocity information. In contrast, HeRCULES combines 4D radar, FMCW LiDAR, and spinning radar, providing enhanced robustness in SLAM across diverse weather, lighting, urban traffic, and dynamic conditions.

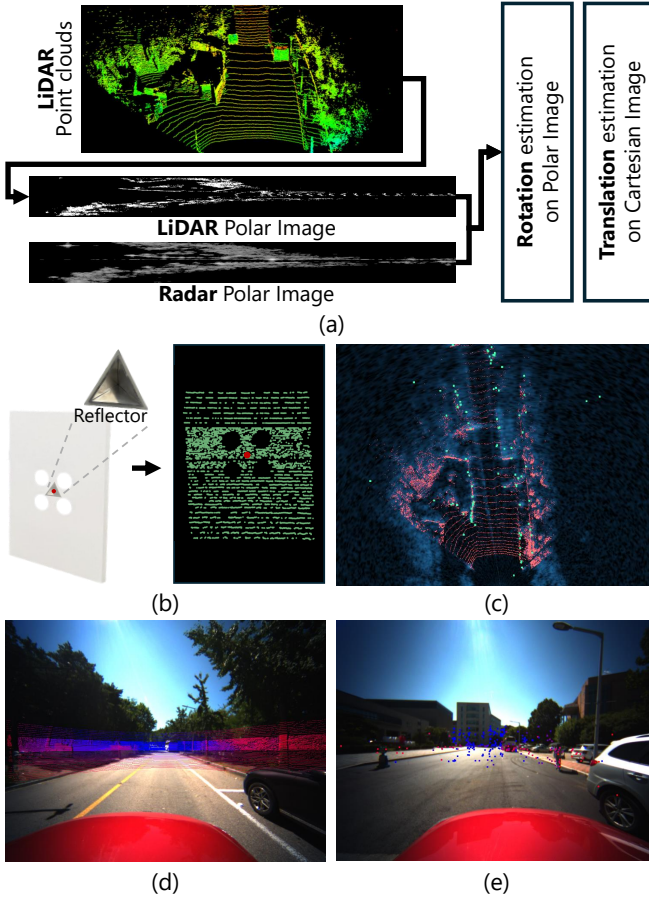[1]https://github.com/robotics-upo/ars548_ros/tree/noetic

Fig. 4: (a) LiDAR - spinning radar extrinsic calibration pipeline. (b) Utilizing the line-index channel. (c) LiDAR points, 4D radar points, and spinning radar points are red, green, and blue. (d) Right camera - LiDAR. (e) Left camera - 4D radar.

III. SYSTEM OVERVIEW

A. System Configuration

The sensor configuration and coordinates of each sensor are illustrated in Fig. 2, and their specifications are detailed in Table. II. The Aeva LiDAR operates with relative velocity settings synchronized to the 4D radar sensor. The Continental radar provides both raw radar point cloud data and filtered object point cloud data via its sensor driver. All sensor data are processed on an industrial PC, the NUVO-9006LP-NX, equipped with an Intel Core i9 processor, 2 TB SSD, and 64 GB DDR5 RAM. The sample data is shown in Fig. 3.

B. Sensor Calibration

1) Extrinsic Calibration of LiDAR - Spinning Radar: We employ the method used in the Boreas dataset [25]. This method determines the rotation $\mathbf{R}_R^L$ and the translation $\mathbf{t}_R^L$ in the xy plane through correlative scan matching with the Fourier-Mellin transform [31]. Specifically, we convert LiDAR point clouds into LiDAR polar images to compare with radar polar images to obtain $\mathbf{R}_R^L$. Then, we utilize Cartesian images to derive $\mathbf{t}_R^L$. To match the field of view (FOV) of the Aeva, we adjust the range and azimuth of the radar images. The calibration pipeline is shown in Fig. 4(a).

TABLE III: OVERVIEW OF SEQUENCES

Sequence	Index	Time	Weather	Length	Loop	Target
Mountain	01	Day	Clear	4 km	2 times	odometry,
	02	Night	Cloud	4 km	2 times	online place recognition,
	03	Day	Snow	3 km	1.5 times	global localization
Library	01	Day	Clear	1.6 km	2 times	odometry,
	02	Night	Cloud	1.6 km	2 times	online place recognition,
	03	Day	Snow	0.8 km	1 time	global localization
Sports Complex	01	Day	Clear	1.4 km	2 times	odometry,
	02	Night	Cloud	0.7 km	1 time	online place recognition,
	03	Day	Snow	1.4 km	2 times	global localization
Parking Lot	01	Day	Clear	0.4 km		
	02	Day	Clear	0.4 km	inter-session	odometry,
	03	Night	Cloud	0.5 km		global localization
	04	Day	Snow	0.4 km		
River Island	01	Day	Clear	4 km		odometry,
	02	Dusk	Cloud	8 km	inter-session	global localization
	03	Day	Cloud	5.8 km		
Bridge	01	Day	Rain	4.9 km	1 time	odometry,
	02	Night	Cloud	4.9 km	1 time	online place recognition
Street	01	Day	Rain	1 km	1 time	odometry
Stream	01	Day	Clear	4.2 km	2 times	odometry,
	02	Night	Cloud	5.5 km	2 times	online place recognition

2) Extrinsic Calibration of LiDAR - 4D Radar - Camera: We utilize the calibration tool [32] for cameras, LiDAR, and radar. This tool jointly calculates relative transformation parameters using a specialized calibration board and reflector. Although we use a solid-state LiDAR instead of a spinning one, we utilize the line-index channel to assess laser depth discontinuity, as illustrated in Fig. 4(b). Unlike Domhof et al. [32], who estimates the reflector position with 2D radar, we can directly obtain the z-value from our 4D radar, resulting in more accurate calibration.

3) Extrinsic Calibration of LiDAR - IMU: We initialize the system using the method proposed by Zhu et al. [33]. This approach was designed for the Livox LiDAR series, so it can be seamlessly applied to our solid-state Aeva LiDAR without requiring specific targets.

4) Calibration Evaluation: The calibration results are shown in Fig. 4(c), Fig. 4(d) and Fig. 4(e).

IV. DESCRIPTION OF HERCULES DATASET

A. Target Environments

This subsection briefly outlines the reasons for selecting the eight target environments depicted in Fig. 5. An overview of the eight sequences is presented in Table. III.

1) Mountain: Mountain captures sequences on Gwanak Mountain, the highest elevation difference among all sequences. The route includes speed bumps and rough roads, causing significant rolling and pitching.

2) Library: Library captures sequences from a long, narrow, one-way path near the library on campus. The path includes steep curves with uphill and downhill sections.

3) Sports Complex: Sports Complex captures sequences around a sports complex, including parking areas and roads with flat, gently sloped, and steep sections. Two loops with an average speed below 30 km/h were recorded during the day and night.

4) Parking Lot: Parking Lot captures sequences from a parking lot with many left turns, recorded on a clear afternoon and at night. While the ground appears flat, slight elevation variations are noted. This sequence has the shortest distance among all.
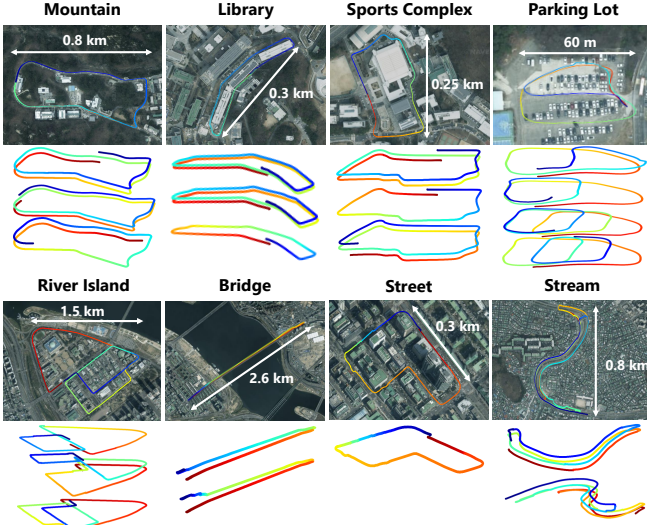
Fig. 5: Trajectory overlaid on satellite maps for each sequence with colors. Red indicates the start, while blue designates the end.

5) River Island: `River Island` captures three sequences for multi-session place recognition with each route uniquely designed. The flat area features various driving paths, including intersections and two-lane one-way roads.

6) Bridge: `Bridge` captures sequences for place recognition research, driven back and forth along a four-lane overpass and the Wonhyo Bridge over the Han River. It includes sequences recorded on a rainy afternoon and cloudy dusk, with an average speed of 60 km/h, and sections featuring traffic congestion in urban environments.

7) Street: `Street` captures a sequence of driving in heavy congestion and rain near IFC Seoul during rush hour. Due to the crowds and numerous vehicles, there are many dynamic objects, leading to frequent stops.

8) Stream: `Stream` captures an S-shaped stream route with one-way roads running along both sides, allowing U-turns via bridges. For place recognition research, intentional revisits were designed, resulting in similar environments.

B. Data Description and Format

The file structure of the HeRCULES dataset is delineated in Fig. 6. The acquisition time of all measurements are stored in `datastamp.csv`. The FMCW LiDAR and 4D radar data are provided in `time.bin`, while the camera data is in `time.png`. For spinning radar data, we support software that converts raw polar images into Oxford-style [22] and Cartesian images. IMU, GPS, and inertial navigation system (INS) data are provided in `.csv`, and calibration information between sensors is available in `.yaml` and `.txt` format. The data types for each sensor are detailed in Table. II.

C. Individual Ground Truth

Before logging each sequence, we ensure that the GNSS solution is fixed and the INS solution has converged. We use Precision Time Protocol (PTP) to synchronize timestamps in Coordinate Universal Time (UTC) across all sensors. However, spatiotemporal discrepancies arise due to differences in sensor mounting positions and data acquisition times.
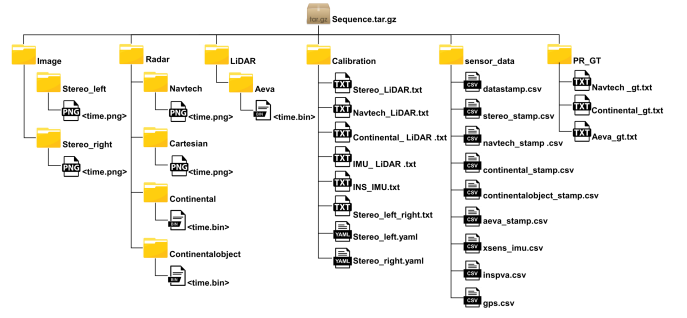

Fig. 6: File structure of the HeRCULES dataset, illustrating the organization of sensor scans, ground truths, calibration, and inertial sensor measurements for each sequence.
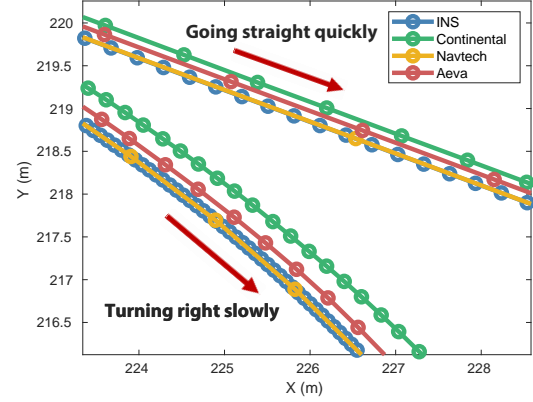

Fig. 7: Ground truth pose for each sensor is overlaid on the path of the `River Island`, illustrating a right turn and a straight drive.

To address this, we provide ground truth poses for each sensor to support place recognition research, handling spatial differences using extrinsic calibration results and temporal differences with B-Spline interpolation [34]. The ground truth is shown in Fig. 7, highlighting the importance of independently deriving ground truth pose for each sensor.

V. EVALUATION OF HeRCULES DATASET

A. SLAM Evaluation

For the SLAM baseline, we use Fast-LIO [35] for LiDAR SLAM, 4DRadarSLAM [11] for 4D radar SLAM, and ORORA [36] for spinning radar SLAM. Fig. 1 shows the mapping results for the `Sports Complex` using ORORA. A comparison of these three baselines on `Sports Complex` and `Library` is shown in Fig. 8 and Table. IV. Absolute Trajectory Error (ATE) is measured in meters, while Relative Pose Error (RPE) is quantified in degrees per meter for rotation (RPE_r) and as a percentage for translation (RPE_t). Among these baselines, the odometry result of Fast-LIO was the most accurate, followed by ORORA and 4DRadarSLAM. The result of 4DRadarSLAM is not as good because the point cloud from the Continental radar we used contains fewer points than the Oculii radar originally used in 4DRadarSLAM. However, there is potential for improvement through preprocessing the raw point cloud. These findings validate that SLAM performance with 4D radar alone is limited on our dataset, highlighting the need for heterogeneous radar SLAM or radar-LiDAR fusion SLAM.

TABLE IV: QUANTITATIVE ANALYSIS: ATE and RPE

Sequence	Fast-LIO			4DRadarSLAM			ORORA		
	ATE_t	RPE_r	RPE_t	ATE_t	RPE_r	RPE_t	ATE_t	RPE_r	RPE_t
Sports Complex 01	10.358	0.950	1.763	64.884	3.926	2.429	9.229	5.909	2.167
Library 01	10.382	0.768	1.805	92.892	11.215	3.477	33.348	5.143	2.045

TABLE V: QUANTITATIVE ANALYSIS: AUC SCORES

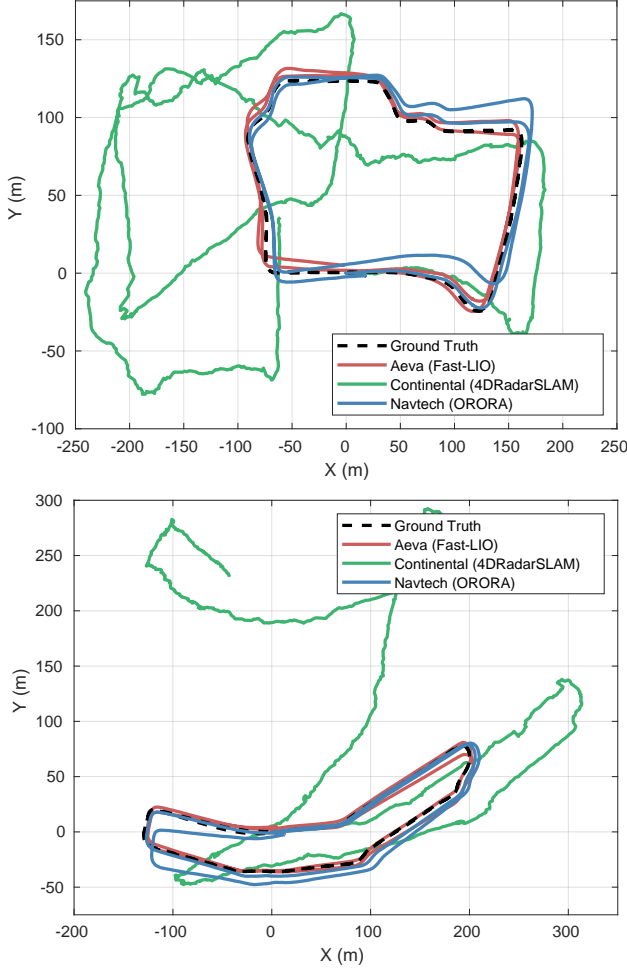| Sequence	Aeva			Continental			Aeva-Continental		
	10 m	15 m	20 m	10 m	15 m	20 m	10 m	15 m	20 m
Sports Complex	0.976	-	-	0.809	-	-	0.401	-	-
Library	0.971	0.975	0.988	0.574	0.584	0.632	0.276	0.296	0.331

Fig. 8: Estimated odometry of Fast-LIO, 4DRadarSLAM and ORORA with the ground truth for `Sports Complex 01` and `Library 01`.

Fig. 9: Place recognition result for `Sports Complex`.

Fig. 10: Place recognition result for `Library`.

B. Place Recognition Evaluation

We use Scan Context [37] for place recognition with both 4D LiDAR and 4D radar. Additionally, we evaluate cross-modal place recognition performance using radar queries on a LiDAR-based database. The experiments utilize `01` sequences as the database and `02` sequences as the query set, with the results shown in Fig. 9. For the `Sports Complex`, a query is considered correct if the top result is within 10 m, indicating accurate recognition of a revisited location or rejection of false positives. The ablation study conducted for the `Library` shows the results for thresholds of 10 m, 15 m, and 20 m in Fig. 10. The AUC scores for the place recognition evaluation are presented in Table. V. These results highlight that 4D LiDAR achieves the highest place recognition performance, while cross-modal recognition between LiDAR and radar is the lowest. This suggests a need for further research in place recognition using heterogeneous sensors, for which HeRCULES offers valuable data.

VI. CONCLUSION

The HeRCULES dataset is a comprehensive benchmark for SLAM and sensor fusion research in autonomous driving, uniquely integrating a diverse sensor suite including 4D radar, spinning radar, FMCW LiDAR, IMU, GPS, and cameras. It is the first public dataset to combine 4D radar, spinning radar, and FMCW LiDAR, offering unique localization, mapping, and place recognition capabilities. Including both 4D radar and FMCW LiDAR supports diverse research in radar-LiDAR fusion SLAM, cross-sensor place recognition, and radar point upsampling. Covering diverse weather, lighting, and traffic conditions with sequences that revisit the same locations, the dataset is ideal for robust place recognition and SLAM evaluation. Additionally, the HeRCULES dataset includes ROS-compatible tools and ground truth pose data for each sensor, facilitating the development of advanced SLAM and localization algorithms. Through benchmark evaluations for SLAM, we identified the limitations of single radar SLAM in various environments, underscoring the need for sensor fusion SLAM research. Additionally, benchmark evaluations for place recognition tasks highlighted the necessity for cross-sensor place recognition research. By offering rich, multi-modal data under varied conditions, HeRCULES sets a new standard for research in autonomous navigation, enabling the creation of next-generation perception systems.

References

[1] K. Harlow, H. Jang, T. D. Barfoot, A. Kim, and C. Heckman, "A new wave in robotics: Survey on recent mmwave radar applications in robotics," *arXiv preprint arXiv:2305.01135*, 2023.

[2] M. Gadd, D. De Martini, and P. Newman, "Look around you: Sequence-based radar place recognition with learned rotational invariance," in *2020 IEEE/ION Position, Location and Navigation Symposium (PLANS)*. IEEE, 2020, pp. 270–276.

[3] Y. S. Park, Y.-S. Shin, and A. Kim, "Pharao: Direct radar odometry using phase correlation," in *2020 IEEE International Conference on Robotics and Automation (ICRA)*. IEEE, 2020, pp. 2617–2623.

[4] H. Jang, M. Jung, and A. Kim, "Raplace: Place recognition for imaging radar using radon transform and mutable threshold," in *2023 IEEE/RSJ International Conference on Intelligent Robots and Systems (IROS)*. IEEE, 2023, pp. 11 194–11 201.

[5] Y. Xia, P. Wang, K. Berntorp, L. Svensson, K. Granström, H. Mansour, P. Boufounos, and P. V. Orlik, "Learning-based extended object tracking using hierarchical truncation measurement model with automotive radar," *IEEE Journal of Selected Topics in Signal Processing*, vol. 15, no. 4, pp. 1013–1029, 2021.

[6] A. Sengupta, L. Cheng, and S. Cao, "Robust multiobject tracking using mmwave radar-camera sensor fusion," *IEEE Sensors Letters*, vol. 6, no. 10, pp. 1–4, 2022.

[7] A. Pearce, J. A. Zhang, R. Xu, and K. Wu, "Multi-object tracking with mmwave radar: A review," *Electronics*, vol. 12, no. 2, p. 308, 2023.

[8] B. Tan, Z. Ma, X. Zhu, S. Li, L. Zheng, S. Chen, L. Huang, and J. Bai, "3-d object detection for multiframe 4-d automotive millimeter-wave radar point cloud," *IEEE Sensors Journal*, vol. 23, no. 11, pp. 11 125–11 138, 2022.

[9] X. Cao, J. Lan, X. R. Li, and Y. Liu, "Extended object tracking using automotive radar," in *2018 21st International Conference on Information Fusion (FUSION)*. IEEE, 2018, pp. 1–5.

[10] Y. Zhuang, B. Wang, J. Huai, and M. Li, "4d iriom: 4d imaging radar inertial odometry and mapping," *IEEE Robot. and Automat. Lett.*, 2023.

[11] J. Zhang, H. Zhuge, Z. Wu, G. Peng, M. Wen, Y. Liu, and D. Wang, "4dradarslam: A 4d imaging radar slam system for large-scale environments based on pose graph optimization," in *2023 IEEE International Conference on Robotics and Automation (ICRA)*. IEEE, 2023, pp. 8333–8340.

[12] X. Li, H. Zhang, and W. Chen, "4d radar-based pose graph slam with ego-velocity pre-integration factor," *IEEE Robotics and Automation Letters*, 2023.

[13] M. Meyer and G. Kuschk, "Automotive radar dataset for deep learning based 3d object detection," in *2019 16th European Radar Conference (EuRAD)*, 2019, pp. 129–132.

[14] J. Rebut, A. Ouaknine, W. Malik, and P. Pérez, "Raw high-definition radar for multi-task learning," in *Proc. IEEE Conf. on Comput. Vision and Pattern Recog.*, June 2022, pp. 17 021–17 030.

[15] A. Palffy, E. Pool, S. Baratam, J. F. Kooij, and D. M. Gavrila, "Multi-class road user detection with 3+ 1d radar in the view-of-delft dataset," *IEEE Robot. and Automat. Lett.*, vol. 7, no. 2, pp. 4961–4968, 2022.

[16] L. Zheng, Z. Ma, X. Zhu, B. Tan, S. Li, K. Long, W. Sun, S. Chen, L. Zhang, M. Wan *et al.*, "Tj4dradset: A 4d radar dataset for autonomous driving," in *Proc. IEEE Intell. Transport. Sys. Conf.* IEEE, 2022, pp. 493–498.

[17] D.-H. Paek, S.-H. Kong, and K. T. Wijaya, "K-radar: 4d radar object detection for autonomous driving in various weather conditions," *Advances in Neural Information Processing Sys. Conf.*, vol. 35, pp. 3819–3829, 2022.

[18] M. Choi, S. Yang, S. Han, Y. Lee, M. Lee, K. H. Choi, and K.-S. Kim, "Msc-rad4r: Ros-based automotive dataset with 4d radar," *IEEE Robot. and Automat. Lett.*, 2023.

[19] J. Zhang, H. Zhuge, Y. Liu, G. Peng, Z. Wu, H. Zhang, Q. Lyu, H. Li, C. Zhao, D. Kircali *et al.*, "Ntu4dradlm: 4d radar-centric multi-modal dataset for localization and mapping," in *Proc. IEEE Intell. Transport. Sys. Conf.* IEEE, 2023, pp. 4291–4296.

[20] X. Zhang, L. Wang, J. Chen, C. Fang, L. Yang, Z. Song, G. Yang, Y. Wang, X. Zhang, and J. Li, "Dual radar: A multi-modal dataset with dual 4d radar for autononous driving," *arXiv preprint arXiv:2310.07602*, 2023.

[21] J. Huai, B. Wang, Y. Zhuang, Y. Chen, Q. Li, Y. Han, and C. Toth, "Snail-radar: A large-scale diverse dataset for the evaluation of 4d-radar-based slam systems," *arXiv preprint arXiv:2407.11705*, 2024.

[22] D. Barnes, M. Gadd, P. Murcutt, P. Newman, and I. Posner, "The oxford radar robotcar dataset: A radar extension to the oxford robotcar dataset," in *Proc. IEEE Intl. Conf. on Robot. and Automat.* IEEE, 2020, pp. 6433–6438.

[23] G. Kim, Y. S. Park, Y. Cho, J. Jeong, and A. Kim, "Mulran: Multimodal range dataset for urban place recognition," in *Proc. IEEE Intl. Conf. on Robot. and Automat.* IEEE, 2020, pp. 6246–6253.

[24] M. Sheeny, E. De Pellegrin, S. Mukherjee, A. Ahrabian, S. Wang, and A. Wallace, "Radiate: A radar dataset for automotive perception in bad weather," in *Proc. IEEE Intl. Conf. on Robot. and Automat.* IEEE, 2021, pp. 1–7.

[25] K. Burnett, D. J. Yoon, Y. Wu, A. Z. Li, H. Zhang, S. Lu, J. Qian, W.-K. Tseng, A. Lambert, K. Y. Leung *et al.*, "Boreas: A multi-season autonomous driving dataset," *Intl. J. of Robot. Research*, vol. 42, no. 1-2, pp. 33–42, 2023.

[26] M. Gadd, D. De Martini, O. Bartlett, P. Murcutt, M. Towlson, M. Widojo, V. Muşat, L. Robinson, E. Panagiotaki, G. Pramatarov *et al.*, "Oord: The oxford offroad radar dataset," *arXiv preprint arXiv:2403.02845*, 2024.

[27] Y. S. Park, Y.-S. Shin, J. Kim, and A. Kim, "3d ego-motion estimation using low-cost mmwave radars via radar velocity factor for pose-graph slam," *IEEE Robotics and Automation Letters*, vol. 6, no. 4, pp. 7691–7698, 2021.

[28] K. Sayyah, R. Sarkissian, P. Patterson, B. Huang, O. Efimov, D. Kim, K. Elliott, L. Yang, and D. Hammon, "Fully integrated fmcw lidar optical engine on a single silicon chip," *Journal of Lightwave Technology*, vol. 40, no. 9, pp. 2763–2772, 2022.

[29] C. Kim, Y. Jung, and S. Lee, "Fmcw lidar system to reduce hardware complexity and post-processing techniques to improve distance resolution," *Sensors*, vol. 20, no. 22, p. 6676, 2020.

[30] Z. Xu, H. Zhang, K. Chen, D. Zhu, and S. Pan, "Fmcw lidar using phase-diversity coherent detection to avoid signal aliasing," *IEEE Photonics Technology Letters*, vol. 31, no. 22, pp. 1822–1825, 2019.

[31] P. Checchin, F. Gérossier, C. Blanc, R. Chapuis, and L. Trassoudaine, "Radar scan matching slam using the fourier-mellin transform," in *Field and Service Robotics: Results of the 7th International Conference*. Springer, 2010, pp. 151–161.

[32] J. Domhof, J. F. Kooij, and D. M. Gavrila, "A joint extrinsic calibration tool for radar, camera and lidar," *IEEE Transactions on Intelligent Vehicles*, vol. 6, no. 3, pp. 571–582, 2021.

[33] F. Zhu, Y. Ren, and F. Zhang, "Robust real-time lidar-inertial initialization," in *2022 IEEE/RSJ International Conference on Intelligent Robots and Systems (IROS)*. IEEE, 2022, pp. 3948–3955.

[34] E. Mueggler, G. Gallego, H. Rebecq, and D. Scaramuzza, "Continuous-time visual-inertial odometry for event cameras," *IEEE Transactions on Robotics*, vol. 34, no. 6, pp. 1425–1440,

2018.

[35] W. Xu and F. Zhang, "Fast-lio: A fast, robust lidar-inertial odometry package by tightly-coupled iterated kalman filter," *IEEE Robotics and Automation Letters*, vol. 6, no. 2, pp. 3317–3324, 2021.

[36] H. Lim, K. Han, G. Shin, G. Kim, S. Hong, and H. Myung, "Orora: Outlier-robust radar odometry," in *2023 IEEE International Conference on Robotics and Automation (ICRA)*. IEEE, 2023, pp. 2046–2053.

[37] G. Kim and A. Kim, "Scan context: Egocentric spatial descriptor for place recognition within 3d point cloud map," in *2018 IEEE/RSJ International Conference on Intelligent Robots and Systems (IROS)*. IEEE, 2018, pp. 4802–4809.